Eur. Phys. J. Special Topics **224**, 3185–3197 (2015)
© EDP Sciences, Springer-Verlag 2015
DOI: 10.1140/epjst/e2015-50086-4

THE EUROPEAN PHYSICAL JOURNAL SPECIAL TOPICS

Regular Article

Self-propulsion of free solid bodies with internal rotors via localized singular vortex shedding in planar ideal fluids

P. Tallapragada[1] and S.D. Kelly[2,a]

[1] Department of Mechanical Engineering, Clemson University, Clemson, USA
[2] Department of Mechanical Engineering and Engineering Science, University of North Carolina at Charlotte, Charlotte, USA

Received 16 April 2015 / Received in final form 2 November 2015
Published online 15 December 2015

Abstract. Diverse mechanisms for animal locomotion in fluids rely on vortex shedding to generate propulsive forces. This is a complex phenomenon that depends essentially on fluid viscosity, but its influence can be modeled in an inviscid setting by introducing localized velocity constraints to systems comprising solid bodies interacting with ideal fluids. In the present paper, we invoke an unsteady version of the Kutta condition from inviscid airfoil theory and a more primitive stagnation condition to model vortex shedding from a geometrically contrasting pair of free planar bodies representing idealizations of swimming animals or robotic vehicles. We demonstrate with simulations that these constraints are sufficient to enable both bodies to propel themselves with very limited actuation. The solitary actuator in each case is a momentum wheel internal to the body, underscoring the symmetry-breaking role played by vortex shedding in converting periodic variations in a generic swimmer's angular momentum to forward locomotion. The velocity constraints are imposed discretely in time, resulting in the shedding of discrete vortices; we observe the roll-up of these vortices into distinctive wake structures observed in viscous models and physical experiments.

1 Introduction

The idealized representation of viscous vortex shedding enables the realization of reduced-order models for diverse biological and biomimetic locomotion systems. Of particular interest to the authors are the shedding of vorticity from the caudal fins of certain fishes, the shedding of vortex rings from the bells of medusan jellyfish, and similar localized phenomena that may be exploited by biologically inspired robotic vehicles for propulsion. In the context of robotics, models of sufficiently low order may be used not only for computationally efficient simulation but also for analytical control design and motion planning.

[a] e-mail: scott@kellyfish.net

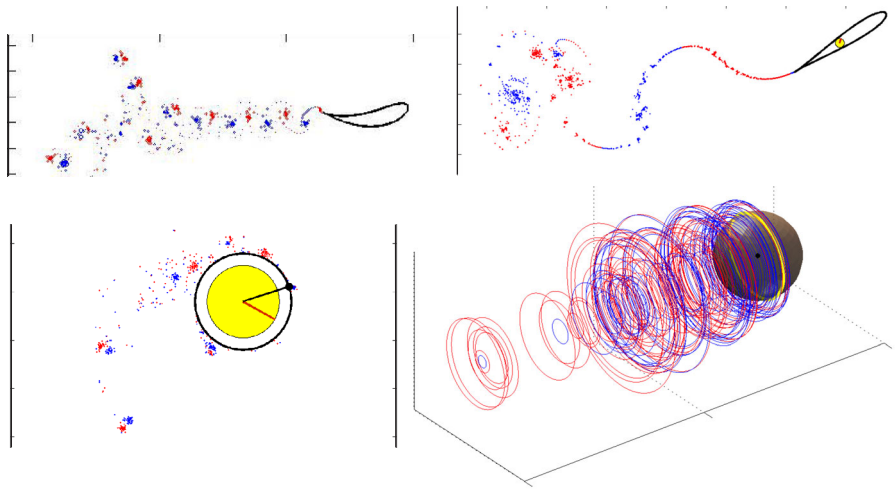

Fig. 1. Still images from simulations of four locomotion systems described in the text. In each case, the body shown accelerates to the right from rest as a result of periodic variations in a single control input. Discrete vortex elements are shaded according to their sign.

Models that represent vortex shedding and vortex-body interactions in terms of inviscid point vortices have a rich history. Early examples of such work include the investigation of wake characteristics for a cylinder started impulsively from rest [1] and the dissipation in energy and vorticity in the near wake for flow past a bluff body [2]. Inviscid vortices appear in models for planar fishlike swimming in [3–5]. The shedding of a vortex wake from a moving boundary is explored in [6,7] using steady-vortex models and in [8–10] using unsteady-vortex models. Additional aspects of dynamic interactions between free bodies and point vortices in inviscid fluids, and elaborations on the preceding work, are considered in [11–17].

Noncanonical Hamiltonian structures have been shown to underpin the interactions of free bodies with singular distributions of vorticity in both two- and three-dimensional ideal fluids [18–21]. The authors and collaborators have constructed a sequence of models for aquatic locomotion systems by augmenting the relevant Hamiltonian equations with mechanisms for momentum-conserving discrete vortex shedding. Figure 1 depicts four such models. At the top left of Fig. 1, a free hydrofoil sheds vorticity from its trailing point as its camber varies sinusoidally. The shape of the foil is realized as the image of a circle under a time-periodic Joukowski transformation. At the top right, the shape of such a foil is frozen with zero camber, but an internal rotor is driven periodically to induce the foil to pivot. In each case, vortex shedding is mediated by the time-periodic application of a Kutta condition at the foil's trailing point, corresponding to the requirement of stagnation at the preimage of this point in the circle plane. The first of these two systems is described in greater detail in [22,23]. The second is detailed in Sect. 2 of the present paper.

At the bottom left of Fig. 1, a vehicle with circular cross section is shown, again driven by an internal rotor. The surface of this vehicle features no cusp; vortex shedding is mediated by the time-periodic requirement of relative stagnation in the physical plane at a chosen surface point. The wake of the vehicle at the top left is characterized by the roll-up of shed point vortices into an inverse Kármán vortex street, which may be regarded as comprising pairs of counter-rotating vortex structures that convey fluid momentum to the rear behind the foil. Vortex structures of alternating sign travel in alternate directions around the vehicle at the bottom left;

the vehicle accelerates to the right as these structures form pairs antipodal to the shedding point. This system is described in greater detail in Sect. 3 of the present paper.

At the bottom right of Fig. 1, a free sphere sheds vorticity according to the time-periodic application of a velocity constraint along a circular contour that moves periodically along the sphere's surface. This constraint requires relative stagnation perpendicular to the contour, which loosely models the undulating lip of a jellyfish bell, and represents a higher-dimensional analogue of the velocity constraint applied to the system at the bottom left. The system at the bottom right is discussed in greater detail in [24].

In terms of the abstract formalism of [20,21], the velocity constraints depicted in Fig. 1 may be associated with group-invariant distributions defined on the corresponding systems' configuration manifolds, and as such may be characterized as holonomic or nonholonomic. Analogies between the dynamics of the systems in Fig. 1 and the dynamics of simple mechanical systems subject to symmetry-breaking constraints translate into analogies in the behavior of these systems under feedback control, a point explored in preliminary form in [25,26].

2 Joukowski foil with an internal rotor

Consider a free hydrofoil surrounded by a fluid of unit density that extends to infinity in all directions. We regard the plane of the fluid and the foil as the complex plane and denote the region occupied by the foil by $\mathcal{B}$. The geometry of the foil is defined by mapping its boundary $\partial\mathcal{B}$ from a circle with radius r_c in the complex plane through a Joukowski transformation

$$z = F(\zeta) = \zeta + \zeta_c + \frac{a^2}{\zeta + \zeta_c}, \tag{1}$$

where ζ_c is complex and a is real. We refer to the ζ plane as the circle plane and to the z plane as the foil plane. For the zero-camber foil shown at the top right of Fig. 1, ζ_c is real. The preimage of the trailing cusp on the foil is given by $\zeta_t = a - \zeta_c$. The transformation is conformal everywhere in the open set $|\zeta_c| > r_c$. The derivative of the transformation

$$F'(\zeta) = 1 - \frac{a^2}{(\zeta + \zeta_c)^2} \tag{2}$$

exists everywhere except at ζ_t.

The free foil has three degrees of freedom; it can translate with velocity $\mathbf{U} = (U_1, U_2)$ and rotate with angular velocity Ω. We suppose the foil to be coupled to a balanced rotor with moment of inertia I_c that has no direct coupling to the fluid, as depicted in yellow in Fig. 1. The rotor is affixed to the foil at the origin of the z plane. The orientation of the rotor relative to the foil as the former spins is given by the angle β.

2.1 Complex potentials

The fluid surrounding the foil is assumed to be ideal almost everywhere, with a singular distribution of vorticity modeled by N point vortices at the points $z_k = F(\zeta_k)$. The strength of the kth vortex is equal to Γ_k in both the ζ plane and the z plane. Following [27], the complex potential $W(z) = w(\zeta)$ may be decomposed in

terms of its dependence on the translation of the foil, the rotation of the foil, and each of the N point vortices in the form

$$w(\zeta) = W(z) = U_1 w_1(\zeta) + U_2 w_2(\zeta) + \Omega w_3(\zeta) + \sum_{k=1}^{N} w_v^k(\zeta).$$

On the boundary of the circle, the real components $\phi_v^k(\zeta)$, $\phi_1(\zeta)$, $\phi_2(\zeta)$, $\phi_3(\zeta)$ of the complex potentials $w_v^k(\zeta)$, $w_1(\zeta)$, $w_2(\zeta)$, $w_3(\zeta)$ satisfy the boundary conditions

$$\nabla\phi_v^k \cdot \mathbf{n} = 0, \qquad \nabla\phi_1 \cdot \mathbf{n} = 0, \qquad \nabla\phi_2 \cdot \mathbf{n} = 0, \qquad \nabla\phi_3 \cdot \mathbf{n} = 0, \tag{3}$$

where $\mathbf{n}$ is a vector normal to the boundary.

The potential functions representing the motion of the foil are given by

$$\begin{aligned}
w_1(\zeta) &= \frac{-r_c^2}{\zeta} + \frac{a^2}{\zeta + \zeta_c}, \\
w_2(\zeta) &= -\imath\left(\frac{r_c^2}{\zeta} + \frac{a^2}{\zeta + \zeta_c}\right), \\
w_3(\zeta) &= -\imath\left(\frac{r_c^2}{\zeta}\left(\zeta_c + \frac{a^2}{\zeta_c}\right) - \left(\frac{a^2\zeta_c}{r_c^2 - |\zeta_c|^2} + \frac{a^2}{\zeta_c}\right)\frac{a^2}{\zeta + \zeta_c}\right).
\end{aligned}$$

According to the *Milne-Thomson circle theorem* [28], the potential function $w_v^k(\zeta)$ due to the vortex at ζ_k is

$$w_v^k(\zeta) = \frac{\Gamma}{2\pi\imath}\left(\log(\zeta - \zeta_k) - \log\left(\zeta - \frac{r_c^2}{\bar{\zeta}_k}\right)\right).$$

The flow represented by $w_v^k(\zeta)$ comprises that induced by the vortex at ζ_k and that induced by an image vortex inside the preimage of the foil. The latter introduces a net circulation around the foil; the development of circulation around the foil through vortex shedding plays a fundamental role in the propulsion mechanism described below.

We assume that each vortex in the foil plane is advected by the flow induced by the remaining $N-1$ vortices, by the N image vortices, and by the motion of the foil, obtained from the potential function

$$W_k(z) = W(z) - \frac{\Gamma}{2\pi\imath}\log(z - z_k).$$

The corresponding motion of the kth vortex in the circle plane is given by

$$\dot{\zeta}_k = \left(\overline{\frac{dW_k}{dz}} - (U_1 + \imath U_2 + \imath\Omega z_k)\right)\frac{1}{F'(\zeta)}.$$

2.2 Conservation of impulse

The dynamic interaction of a free body with a system of point vortices in a planar ideal fluid is governed by a system of noncanonical Hamiltonian equations belonging to the class of *Lie-Poisson equations* [29]. If the linear and angular impulse in the

system are both zero initially, they will remain zero [27]; it was shown in [20] that the Lie-Poisson equations in this case take the form

$$\left(\frac{d}{dt} + \Omega\times\right)\mathbf{L} = 0, \qquad \frac{d\mathbf{A}}{dt} + \mathbf{V}\times\mathbf{L} = 0.$$

Here $\mathbf{L}$ and $\mathbf{A}$ are the linear and angular impulse in foil-fixed coordinates and the linear impulse is the sum

$$\mathbf{L} = \mathbf{MV} + \mathbf{L}_v$$

of the impulse due to the motion of the foil and the impulse due to the vortices. The foil's effective mass $\mathbf{M}$ includes both real and added mass. If $\mathbf{r} = (\mathrm{Re}(z), \mathrm{Im}(z))$ and $\mathbf{n_b}$ is the normal vector on $\partial\mathcal{B}$ pointing into the fluid, then

$$\mathbf{L}_v = \oint_{\partial\mathcal{B}} \mathbf{r}\times(\mathbf{n_b}\times\nabla\phi_v)ds + \sum_{k=1}^{N} \Gamma_k \mathbf{r}_k \times \mathbf{e}_3$$

and

$$\mathbf{A} = -\frac{1}{2}\sum_{k=1}^{N}\Gamma_k||\mathbf{r}_k||^2 - \frac{1}{2}\oint_{\partial\mathcal{B}}||\mathbf{r}||^2(\mathbf{n_b}\times\nabla\phi_b + \mathbf{n_b}\times\nabla\phi_v)ds. \tag{4}$$

It's demonstrated in [20,22] that (4) can be simplified considerably to obtain a conservation law of the form

$$\mathbf{I}\begin{pmatrix} V_x \\ V_y \\ \Omega \end{pmatrix} + \begin{pmatrix} \mathbf{L_v} \\ \mathbf{A_v} \end{pmatrix} = \begin{pmatrix} \mathbf{R}^T\mathbf{L}_0 \\ \mathbf{A} - I_c\dot{\beta} \end{pmatrix}, \tag{5}$$

where $\mathbf{L}_0$ is the linear impulse of the system in spatially fixed coordinates, $\mathbf{R}$ is the rotation matrix that transforms body-fixed coordinates to spatially fixed coordinates, $\mathbf{U} = \mathbf{RV}$, and $\mathbf{I}$ is the total effective inertia tensor for the body. The term $I_c\dot{\beta}$ has been added to right-hand side of (5) to account for the spinning of the rotor. The linear impulse $\mathbf{L_v}$ and angular impulse $\mathbf{A_v}$ are functions of the positions of the vortices alone and do not depend on their velocity. They are given by

$$\mathbf{L_v} = -\sum_{k=1}^{N}\frac{\Gamma_k}{2\pi\imath}\left(\zeta_k - \frac{r_c^2}{\bar{\zeta}_k}\right)$$

and

$$\mathbf{A_v} = \mathrm{Im}\left(\frac{\imath}{4\pi}\sum_{k=1}^{N}\Gamma_k\left(r_c^2 + |\zeta_c|^2 + \frac{2r_c^2}{\zeta_k}\left(\zeta_c + \frac{a^2}{\zeta_c}\right)\right.\right.$$
$$\left.\left. - \frac{2a^2(r_c^2 - |\zeta_c|^2)}{\zeta_c(\zeta_k + \zeta_c)} + \frac{a^4(\zeta_k - \zeta_c)}{(r_c^2 - |\zeta_c|^2)(\zeta_k + \zeta_c)}\right)\right) - \frac{1}{2}\sum_{k=1}^{N}\Gamma_k|z_k|^2.$$

2.3 Vortex shedding

The fluid velocity at any point away from a vortex in the circle plane is given by

$$\dot{\zeta} = \left(\overline{\frac{dW}{dz}} - (U_1 + \imath U_2 + \imath\Omega z)\right)\frac{1}{F'(\zeta)}.$$

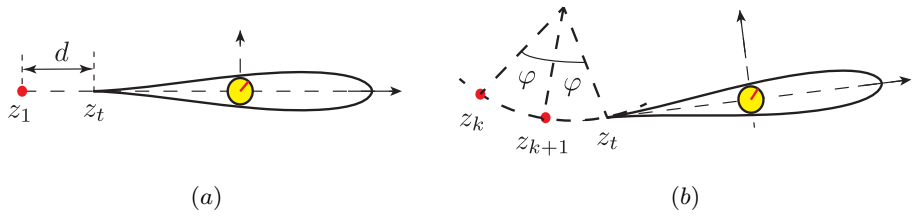

Fig. 2. The placement of (a) the first shed vortex and (b) subsequent shed vortices.

The boundary conditions (3) allow fluid to slip along the circle and foil, but the cusp on the foil corresponds to a singularity of the Joukowski transformation. The derivative $F'(\zeta)$ vanishes there, causing the velocity of the fluid in the circle plane to become undefined. The *Kutta condition* requires that at the preimage ζ_t of the foil's trailing cusp,

$$\left.\frac{dw(\zeta)}{d\zeta}\right|_{\zeta=\zeta_t} = 0.$$

In simulating the fluid-foil system, we enforce the Kutta condition at frequent regular intervals in time by permitting the shedding of new vortices from the cusp. We enforce the additional requirement that the total impulse in the system be preserved through each shedding event by altering the momentum of the foil impulsively at the same time that we fix the strength of each new vortex and its initial position in the fluid near the cusp. In particular,

$$\mathbf{I}\begin{pmatrix}\Delta V_x\\ \Delta V_y\\ \Delta\Omega\end{pmatrix} + \Gamma_{N+1}\begin{pmatrix}\Delta\mathbf{L}_v\\ \Delta\mathbf{A}_v\end{pmatrix} = 0,$$

where $(\Delta V_x, \Delta V_y, \Delta\Omega)$ represent the discrete changes in the foil's velocity associated with a shedding event, Γ_{N+1} is the strength of the newly shed vortex, and $(\Delta\mathbf{L}_v, \Delta\mathbf{A}_v)$ are the changes in the fluid impulse that would correspond to the introduction of a vortex of unit circulation.

The initial location of each newly shed vortex and the shedding frequency can be chosen independently. We make the former choice according to a method employed in [3,5,23]. The first shed vortex is placed an arbitrary small distance d from the trailing edge of the foil along a line tangent to the cusp as shown in Fig. 2(a). For the simulations in the present paper, z_1 is initially $1.01z_t$. When k vortices are present in the wake, the $(k+1)$th vortex is placed on a circular arc joining the kth vortex and the foil's trailing edge, midway between the two, as shown in Fig. 2(b).

To determine an appropriate time interval Δt to separate vortex shedding events, a sequence of simulations corresponding to a reference motion of the foil was performed in which Δt was decreased gradually from 10^{-2} and resulting variations in the foil's predicted dynamics were assessed. Figure 3 depicts the outcome of a sequence of simulations in which Δt decreases from 10^{-2} to 10^{-4}. The foil's dynamics appear to converge to a stable limit; the trajectory represented in Fig. 3 is nearly indistinguishable for different values of $\Delta t \leq 10^{-3}$. For the simulations depicted in the present paper, Δt was assigned the value 10^{-3} to minimize computational cost within the stable range.

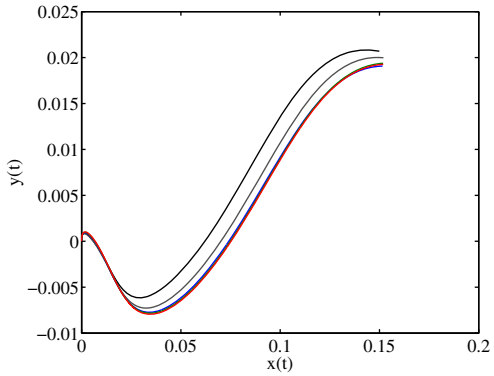

Fig. 3. Trajectory of the foil during a single complete period of rotor oscillation, corresponding to the time interval $0 < t < 0.62$, for five different choices of the fixed interval Δt between vortex shedding events. As this interval decreases through the sequence $\Delta t = 10^{-2}$ (black), $\Delta t = 0.5 \times 10^{-2}$ (grey), $\Delta t = 10^{-3}$ (blue), $\Delta t = 0.5 \times 10^{-3}$ (green), $\Delta t = 10^{-4}$ (red), the trajectories become indistinguishable on the scale of the plot.

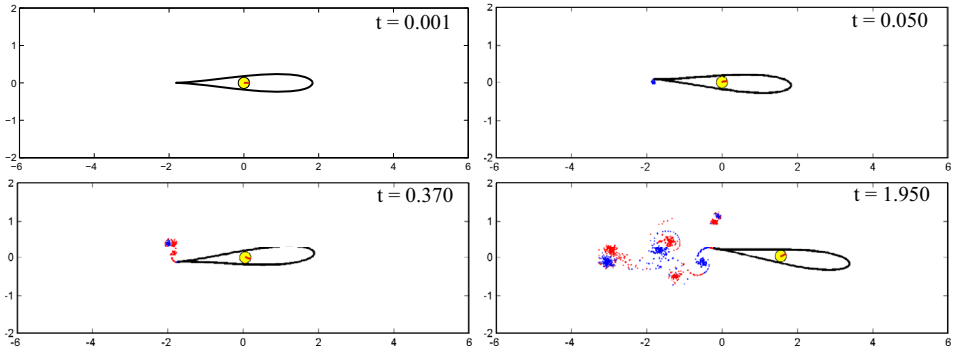

Fig. 4. Acceleration of the foil from rest when the rotor angle varies as $\beta = \frac{\pi}{6} \sin 10t$.

2.4 Forward propulsion

We now demonstrate by solving the equations above numerically that sinusoidal oscillations in the rotor angle induce the foil to accelerate from rest in the forward direction. Figure 4 depicts the configuration of the system at a sequence of four instants in time for the case in which $\beta = \frac{\pi}{6} \sin 10t$. Reversals in the orientation of the vortices being shed occur roughly concurrently with reversals in the rotor's direction of rotation. The system is shown at rest, after the first cluster of vortices with positive (counterclockwise) orientation have been shed, after the first cluster of vortices with negative orientation have been shed, and after three pairs of clusters of vortices with positive and negative circulation have been shed. The fourth panel demonstrates the initial formation of the familiar inverse Kármán vortex wake as a byproduct of the model's dynamics. We note that this wake roll-up can cause the spacing between individual vortices to become very small; regularization methods like δ-regularization [30,31] may become necessary to reproduce this phenomenon with higher fidelity.

Figure 5 depicts the configuration of the system at a sequence of four instants in time for the case in which $\beta = \frac{\pi}{2} \sin 50t$. Increasing the amplitude and frequency of the rotor's oscillation to this extent increases the foil's translational acceleration while decreasing the amplitude of the corresponding variations in the foil's instantaneous

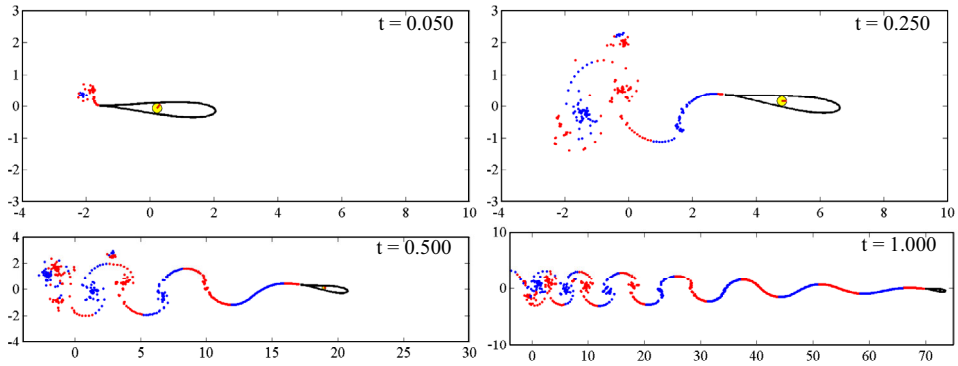

Fig. 5. Acceleration of the foil from rest when the rotor angle varies as $\beta = \frac{\pi}{2} \sin 50t$.

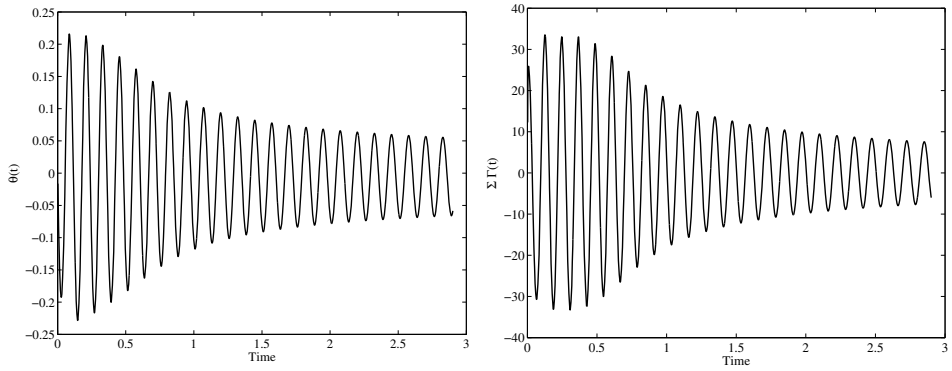

Fig. 6. The foil's heading (left, in radians) and the total shed vorticity (right) as functions of time when $\beta = \frac{\pi}{2} \sin 50t$.

heading. Figure 6 depicts the heading angle θ and the total shed vorticity as functions of time for the simulation in Fig. 5.

2.5 Feedback control of the foil's heading

The problem of steering the foil in the plane by varying the rotor angle β is a problem in underactuated control. The single input to the system provides insufficient actuation to manipulate the foil's three degrees of freedom independently, but it's possible to control the foil's heading, and heading adjustments naturally generate forward propulsion. In [26], the authors and collaborators considered the problem of steering an analogous wheeled vehicle in the plane using a solitary internal rotor for actuation, and it was found that the vehicle's asymptotic heading and asymptotic translational speed could be controlled simultaneously using a simple proportional controller for heading regulation. This controller incorporated a scalar gain but guaranteed asymptotic convergence of the vehicle's heading to a desired value regardless of the value of the gain. The vehicle's asymptotic forward speed, meanwhile, was a monotonic function of the gain.

We demonstrate here that a feedback controller only slightly more complicated than that in [26]–in this case, a *PID controller* rather than a *P controller*–is sufficient to regulate the heading of the foil. We anticipate that variability of the gains in the

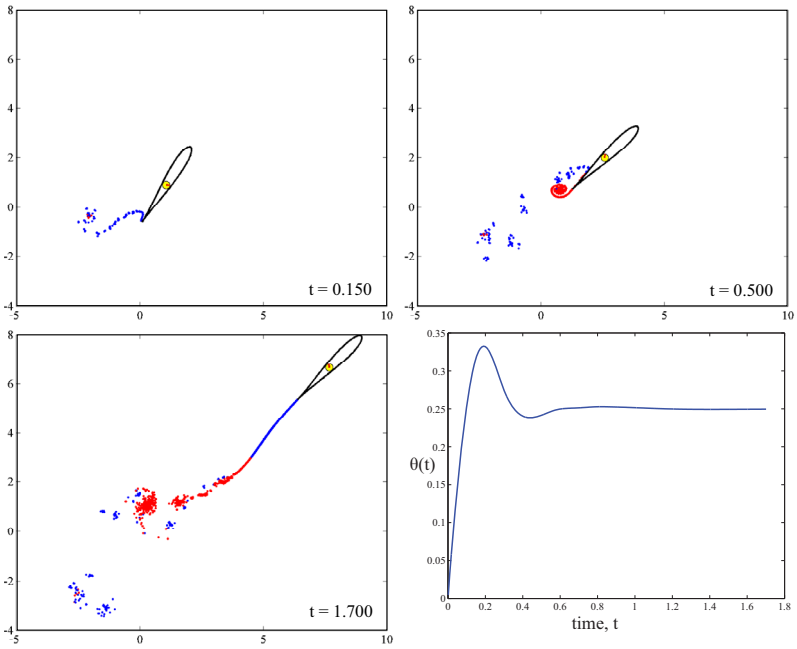

Fig. 7. Reorientation of the foil from $\theta = 0$ to $\theta_d = \frac{\pi}{4}$ via the feedback law (6). The bottom right panel depicts θ (in multiples of π radians) as a function of time.

present controller afford additional authority over the translational speed resulting from a heading adjustment.

We consider the situation in which the foil is initially at rest and the control objective is to change the foil's heading from $\theta = 0$ to $\theta = \theta_d$. To achieve this change, the rotor is driven such that

$$\dot{\beta}(t) = K_p(\theta(t) - \theta_d) + K_i \int_0^t (\theta(\tau) - \theta_d)d\tau + K_d\dot{\theta}(t), \tag{6}$$

with the gains $K_p = 100$, $K_i = 1$, and $K_d = 0.5$ chosen to ensure rapid convergence to the desired heading. Figures 7 and 8 depict the evolution of the system when $\theta_d = \pi/4$ and $\theta_d = \pi/3$, respectively. In each case the foil initially overshoots the desired heading but recovers quickly thereafter.

3 Circular cylinder with an internal rotor

We now describe a system that's more primitive and arguably less physical than the system detailed in Sect. 2, but that demonstrates the universality of phenomena like the rollup and pairing of vortex structures in propulsive planar wakes. Recall that the Kutta condition was introduced to the model in Sect. 2 to address a singularity that arose in the derivative of the Joukowski transformation for generic values of the parameters a and ζ_c. If these parameters are varied smoothly to zero, the Joukowski transformation becomes the identity and the singularity vanishes.

For the circular Joukowski foil arising in this case–referred to hereafter as a cylinder rather than a foil–we can introduce a mechanism for vortex shedding by requiring relative stagnation of the fluid at a certain point in the physical plane rather than

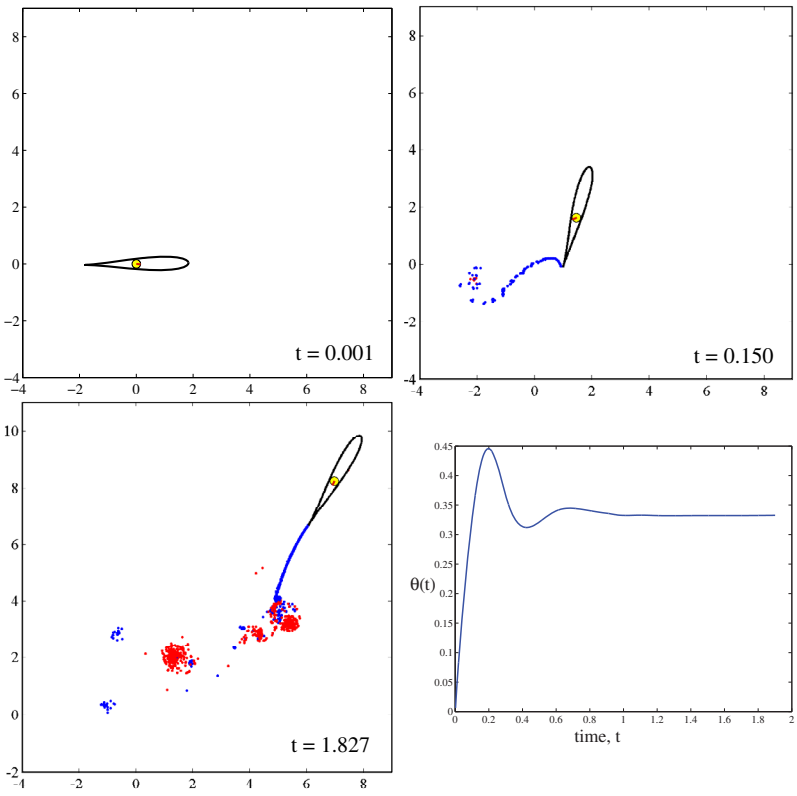

Fig. 8. Reorientation of the foil from $\theta = 0$ to $\theta_d = \frac{\pi}{3}$ via the feedback law (6). The bottom right panel depicts θ (in multiples of π radians) as a function of time.

the preimage plane. Such a point might represent a small but sharp protrusion on the cylinder's otherwise smooth surface. As was the case for the foil with an internal rotor, the cylinder with an internal rotor can propel itself from rest in an ideal fluid only if vortex shedding is permitted.

3.1 Equations of motion

Simplification of the Joukowski transformation relative to the general case considered in Sect. 2 simplifies equalities like (4), in which the contour integral is now zero, substantially. As before, we suppose the cylinder to interact freely with vortices in the fluid according to the conservation of total linear and angular impulse, and we constrain the mechanism whereby new vortices are shed to respect this principle. New vortices are introduced to the fluid adjacent to a point (x_p, y_p) on the cylinder's surface at regular intervals to force relative stagnation there; the circulation around the cylinder changes with each shedding event and the cylinder's velocity is amended discretely to compensate for the impulse of each new vortex.

Suppose N vortices with strengths Γ_k are present at the points $\mathbf{r}_k$ prior to a shedding event, and let the linear and angular impluse due to these vortices be (P_{xN}, P_{yN}) and A_N, respectively. Let the tangential velocity at $\mathbf{r}_p = (x_p, y_p)$ due to these vortices be $u_{tN}(\mathbf{r}_p)$ and let the tangential velocity induced at this point by a vortex of unit circulation at (x_v, y_v) be $\Delta u(\mathbf{r}_p)_t$. With the introduction of a new vortex with

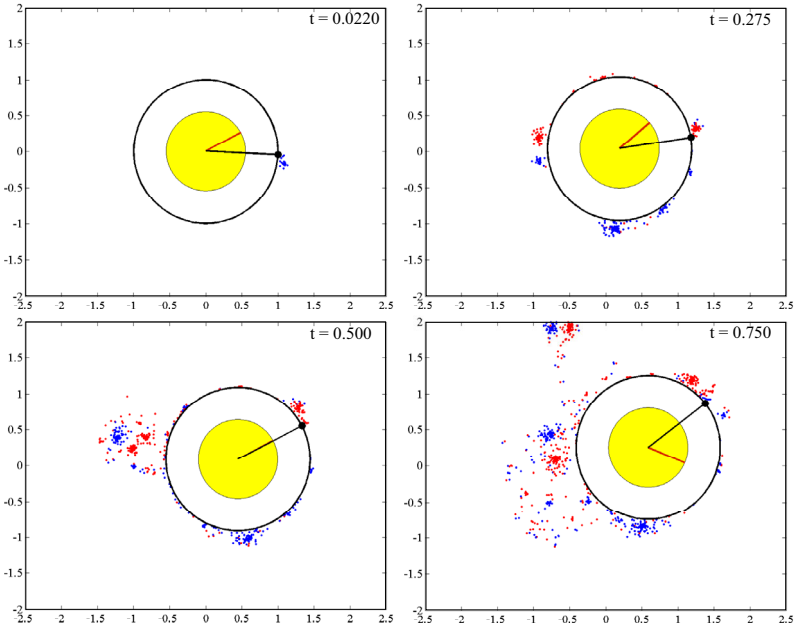

Fig. 9. Acceleration of the cylinder from rest when the rotor angle varies as $\beta = 2\sin 30t$.

strength Γ_{N+1} at (x_v, y_v), the velocity of the cylinder is amended to (U_x^+, U_y^+, Ω^+); these quantities are determined by the equality

$$\begin{pmatrix} \Delta u(\mathbf{r}_p)_t & k_1 & k_2 & -a \\ \Delta P_x & M & 0 & 0 \\ \Delta P_y & 0 & M & 0 \\ \Delta A & 0 & 0 & (I_1 + I_2) \end{pmatrix} \begin{pmatrix} \Gamma_{N+1} \\ U_x^+ \\ U_y^+ \\ \Omega^+ \end{pmatrix} = \begin{pmatrix} -u_{tN}(\mathbf{r}_p) \\ L_x - P_{xN} \\ L_y - P_{yN} \\ A - A_N - I_2\dot{\beta} \end{pmatrix}$$

with $k_1 = \frac{\partial \phi_1}{\partial x}(\cos\theta - \sin\theta) + \sin\theta$ and $k_2 = \frac{\partial \phi_2}{\partial y}(\cos\theta + \sin\theta) - \cos\theta$. The quantities I_1 and I_2 denote the moments of inertia of the cylinder and the rotor, respectively, about their shared center.

3.2 Simulation results

As was the case for the foil in Sect. 2, the cylinder translates when oscillations in the orientation of the internal rotor induce the shedding point on the cylinder's surface to move relative to the fluid, but we observe both qualitative and quantitative differences distinguishing the behavior of the two systems. A qualitative difference visible in Fig. 1 and in Fig. 9 is that the cylinder is propelled, in the net, toward the shedding point on its surface and not away from it. Shed vortices don't move away from the cylinder's surface but cling to it; clusters of vortices with opposite sign migrate around the cylinder in opposite directions and meet to form pairs to the cylinder's left. These pairs then separate from the cylinder, carrying fluid momentum to the left and inducing the cylinder to move right, but do not assemble into the vortex street of Fig. 5.

A quantitative difference between the acceleration of the cylinder and that of the foil is apparent in Fig. 9, which depicts the evolution of the system when $\beta = 2\sin 30t$. The oscillations of the rotor are larger in amplitude than those depicted in

Figs. 4 and 5 and relatively rapid, yet the displacement of the cylinder after several oscillations is relatively small.

4 Conclusions

Localized velocity constraints can be used to represent conditions for localized vortex shedding in otherwise inviscid models for diverse fluid-body interactions. The imposition of such constraints discretely in time in an impulse-conserving way is compatible with existing Hamiltonian formalism for problems involving the interactions of bodies with discrete distributions of vorticity, and simulations based on models constructed in this way are qualitatively consistent with the observed behavior of hydrofoils shedding vorticity in real fluids. In this paper, we've described two models for free bodies shedding discrete vorticity in accordance with localized velocity constraints and highlighted some of their similarities and differences. We've supposed each body to be coupled to an actuated internal rotor as a source of control and explored both rectilinear propulsion and steering as control objectives. We've alluded to a fundamental link between the systems considered herein and other mechanical control systems in which nonintegrable velocity constraints play an essential role; this link will be explored in detail in a forthcoming paper.

The present paper suggests several additional avenues for future work. In each of the models we've presented, for instance, vortex shedding has been constrained to a single body-fixed point, but the underlying methodology is compatible with the imposition of shedding conditions at any finite number of points. The basic analogy to fishlike swimming suggested by the morphology of the hydrofoils in Fig. 1 could be developed with the addition of shedding points representing pectoral fins; the introduction of control authority to mediate shedding from these points would enable the computational study of multimodal propulsion and steering akin to that demonstrated by real fish. Models for the dynamic interactions of multiple fish could in turn be developed using more sophisticated conformal maps and recently developed methods for realizing complex potentials appropriate to vortex dynamics in multiply connected domains [32].

The development of biomimetic aquatic vehicles is motivated in part by the efficiency with which aquatic organisms can propel themselves and maneuver. The prospect of linking the models from the present paper more directly to biological systems suggests an investigation of the efficiency of the systems considered in Sects. 2 and 3. The simulations we've presented represent parametric choices that illuminate qualitative features of these systems but are neither optimized for propulsion nor suggested by specific biological data. At least two notions of efficiency are appropriate for systems like these: one based on the degree of actuator movement associated with a given maneuver and one based on the energetic cost of actuator movement. The latter may be more meaningful from the standpoint of robotic vehicle design, but the models presented herein–involving no calculation of forces or moments–accommodate the former more directly. The present models allow direct assessment, however, of notions from the biomechanics literature like that of a locally optimal *Strouhal number* for forward swimming [33]. The authors intend to address this topic in a forthcoming paper.

References

1. T. Sarpkaya, J. Fluid Mech. **68**, 109 (1975)
2. P.G. Saffman, J.C. Schatzman, J. Fluid Mech. **122**, 467 (1982)

3. K. Streitlien, Ph.D. thesis, Massachusetts Institute of Technology, 1994
4. R.J. Mason, J.W. Burdick, Proc. IEEE Int. Conf. Robot. Autom., 1999
5. R.J. Mason, Ph.D. thesis, California Institute of Techn., 2002
6. M.A. Jones, M.J. Shelley, J. Fluid Mech. **540**, 393 (2005)
7. S. Alben, M.J. Shelley, Phys. Rev. Lett. **100**, 074301 (2008)
8. S. Michelin, S.G.L. Smith, Theor. Comput. Fluid Dyn. **23**, 127 (2009)
9. S. Michelin, S.G.L. Smith, Theor. Comput. Fluid Dyn. **24**, 195 (2010)
10. A. Ysasi, E. Kanso, P.K. Newton, Phys. D **240**, 1574 (2010)
11. J. Koiller, Phys. Lett. A **120**, 391 (1987)
12. J. Roenby, H. Aref, Proc. Royal Soc. London A **466**, 1871 (2010)
13. S. Alben, J. Fluid Mech. **635**, 27 (2009)
14. J. Vankerschaver, E. Kanso, J.E. Marsden, J. Geom. Mech. **1**, 227 (2009)
15. J. Vankerschaver, E. Kanso, J.E. Marsden, Regular and Chaotic Dyn. **15**, 606 (2010)
16. E. Kanso, Theor. Comput. Fluid Dyn. **24**, 201 (2010)
17. J. Roenby, H. Aref, J. Fluids Struct. **27**, 768 (2011)
18. B.N. Shashikanth, J.E. Marsden, J.W. Burdick, S.D. Kelly, Phys. Fluids **14**, 1214 (2002)
19. A.V. Borisov, I.S. Mamaev, S.M. Ramodanov, Regular Chaotic Dyn. **8**, 449 (2003)
20. B.N. Shashikanth, Regular Chaotic Dyn. **10**, 1 (2005)
21. B.N. Shashikanth, A. Sheshmani, S.D. Kelly, J.E. Marsden, Theor. Comput. Fluid Dyn. **22**, 37 (2008)
22. H. Xiong, Ph.D. thesis, University of Illinois at Urbana-Champaign, 2007
23. S.D. Kelly, H. Xiong, Theor. Comput. Fluid Dyn. **24**, 45 (2010)
24. P. Tallapragada, S.D. Kelly, Regular Chaotic Dyn. **18**, 21 (2013)
25. M.J. Fairchild, P.M. Hassing, S.D. Kelly, P. Pujari, P. Tallapragada, Proc. ASME Dyn. Syst. Control Conf. (2011)
26. S.D. Kelly, M.J. Fairchild, P.M. Hassing, P. Tallapragada, Proc. Amer. Control Conf. (2012)
27. S.H. Lamb, Hydrodyn. (Dover, 1945)
28. L.M. Milne-Thomson, Theor. Hydrodyn. (Dover, 1996)
29. J.E. Marsden, T.S. Ratiu, *Introduction to Mechanics and Symmetry*, 2nd edn. (Springer-Verlag, 1999)
30. R. Krasny, J. Fluid Mech. **184**, 123 (1987)
31. R. Krasny, Fluid Dyn. Res. **3**, 93 (1988)
32. D. Crowdy, Theor. Comput. Fluid Dyn. **24**, 9 (2010)
33. M.S. Triantafyllou, G.S. Triantafyllou, Sci. Amer. **272**, 64 (1995)